

Liposome characterization with fluorescence cumulant analysis

Joseph E. Reiner,¹ Andreas Jahn,¹ Laurie E. Locascio,²
Michael Gaitan,¹ John J. Kasianowicz¹

¹NIST, Semiconductor Electronics Division, EEEL, Gaithersburg, MD 20899 USA

²NIST, Biochemical Science Division, CSTL, Gaithersburg, MD 20899 USA

(p) 001-301-975-4358, email: joseph.reiner@nist.gov

ABSTRACT

Liposomes are self-assembled spherical vesicles comprised of a lipid bilayer membrane that segregates an internal aqueous environment from an external aqueous environment. These nanometer-scale structures have demonstrated potential for targeted drug delivery applications. For liposomes to be useful *in vivo*, the liposome size and dosage of molecules contained within them needs to be controlled. We present here a fluorescence-based technique for characterizing the relative encapsulation efficiency, leakage rate, and shelf life of liposome formulations. We report results from three different liposome solutions over a period of two months that show the liposome brightness remains stable while the background dye concentration increases. These parameters may prove useful for optimizing the liposome formation process.

Keywords: nanotechnology, biosystems and health, liposomes, microfluidics, fluorescence correlation spectroscopy, fluorescence cumulant analysis

1. INTRODUCTION

Liposomes are a promising tool for drug delivery applications provided one can control the size distribution and encapsulation efficiency of a liposome mixture. Characterizing these mixtures has proven to be a difficult problem. Liposome formation techniques rely on the mixing of two immiscible phases: either liquid-liquid or liquid-solid. Mixing of these phases often occurs in containers with centimeter length scales where mechanical and/or chemical force fields are very heterogeneous, thus, leading to liposome solutions with large distributions in size and lamellarity. A homogeneous liposome population is only obtained after additional, often disruptive, post-processing procedures; i.e. sonication or membrane extrusion. Our group has previously reported a novel technique for creating liposomes using flow focusing in a microfluidic channel.¹ This technique creates a population of liposomes with a narrow size distribution, without the need for a post-processing step; however, further characterization work is required for these liposome samples.

Single molecule fluorescence detection provides a means for analyzing liposome mixtures where liposome sizes are well below the diffraction limit of a fluorescence microscope. A high numerical aperture microscope objective focuses laser light down to a femtoliter-sized volume that enables single fluorescent molecule detection. The random diffusion of single molecules through the focal volume creates bursts of emitted photons which are analyzed with fluorescence fluctuation spectroscopy (FFS). Previous work combining fluorescence studies with liposome characterization have relied on fluorescence correlation spectroscopy (FCS)^{2,3} and fluorescence intensity distribution analysis (FIDA).³ Here we use another technique known as fluorescence cumulant analysis (FCA)⁴ to analyze liposome mixtures with encapsulated fluorescent dye.

A confocal microscope is calibrated for single molecule detection by measuring the fluorescence from a solution containing a single species of dye molecule. This same dye is encapsulated into nanometer-sized

liposomes, and the first three cumulants of the photon probability distribution function (PDF) are measured. The cumulants provide estimates of the average liposome brightness, the concentration of background dye, and the concentration of liposomes. Over a two-month period these three parameters provided the long-term stability of the liposomes and the leakage rate of dye across the lipid bilayer membrane.

2. THEORY

2.1 Fluorescence cumulant analysis

Consider a tightly focused laser beam that creates a fluorescence excitation volume, $I(r)$, that is much smaller than the total sample volume. The sample contains k different, non-interacting, fluorescent species each having a concentration and molecular brightness, given by c_k and q_k respectively. In the absence of shot-noise, the fluorescent molecules interact with the laser which results in an ideal fluorescence intensity, Φ . Molecules diffuse randomly throughout the excitation volume which makes Φ a random variable. Therefore, we measure the mean, $\langle \Phi \rangle$ and fluctuations about this mean, $\Delta\Phi = \Phi - \langle \Phi \rangle$ where $\langle \rangle$ represents a temporal average. The first three cumulants of Φ are related to c_k and q_k by⁵

$$\langle \Phi \rangle = \chi_1 \sum_k q_k c_k, \quad (1)$$

$$\langle (\Delta\Phi)^2 \rangle = \chi_2 \sum_k q_k^2 c_k, \quad (2)$$

$$\langle (\Delta\Phi)^3 \rangle = \chi_3 \sum_k q_k^3 c_k, \quad (3)$$

where $\chi_n = \int (W(r))^n d^3r$. The fluorescence intensity distribution, $W(r)$, depends on the excitation and collection intensity profiles of the microscope.

The fluorescence is measured by counting the number of photons arriving at a detector during an integration time, T . We assume that the integration time is small enough so that changes in a particle's position over that period can be neglected.⁶ The measured fluorescence introduces a shot noise contribution to the ideal fluorescence. A relation between the moments of the ideal and measured fluorescence is given by,⁵

$$\langle (\Phi)^n \rangle = \langle P! / (P - n)! \rangle \quad (4)$$

where P is the number of photons detected per integration time. $\langle P^n \rangle$ is the n^{th} moment of the measured fluorescence. From eq. 4, the first three cumulants of the ideal and measured fluorescence are related as:

$$\langle \Phi \rangle = \langle P \rangle \quad (5)$$

$$\langle (\Delta\Phi)^2 \rangle = \langle (\Delta P)^2 \rangle - \langle P \rangle \quad (6)$$

$$\langle(\Delta\Phi)^3\rangle = \langle(\Delta P)^3\rangle - 3\langle(\Delta P)^2\rangle + 2\langle P\rangle. \quad (7)$$

Equations 1-3 relate the experimental parameters c_k and q_k to the ideal fluorescence and eqs. 5-7 connect the ideal and observed fluorescence. Combining eqs. 1-3 with eqs. 5-7 allows for the extraction of the relative brightness and absolute concentrations of a binary mixture of fluorescent particles from measurements of $\langle P \rangle$, $\langle(\Delta P)^2\rangle$, and $\langle(\Delta P)^3\rangle$.

The spatial profile functions, χ_n , are absorbed into the c and q parameters with the following substitutions,⁴

$$a = \frac{\chi_1^2}{\chi_2}, \quad (8)$$

$$x_k = \frac{\chi_2}{\chi_1} q_k, \quad (9)$$

$$b = \frac{\chi_2^2}{\chi_1\chi_3}, \quad (10)$$

where a can be thought of as the observation volume, x_k is the brightness of the k^{th} molecular species in photon counts per unit time, and b is a dimensionless geometric factor. Substituting eqs. 8-10 into eqs. 1-3 leads to expressions linear in ac which is equal to N , the average number of particles in the observation volume,

$$\langle P \rangle = \sum_k N_k x_k, \quad (11)$$

$$\langle(\Delta P)^2\rangle - \langle P \rangle = \sum_k N_k x_k^2, \quad (12)$$

$$\langle(\Delta P)^3\rangle - 3\langle(\Delta P)^2\rangle + 2\langle P \rangle = \frac{1}{b} \sum_k N_k x_k^3. \quad (13)$$

Specifically, our system is calibrated by determining the cumulants of the photon PDF for a known concentration of sulforhodamine B (SRB) dye in water. From this, we extract the brightness per molecule x_{SRB} and the geometric parameter b . Equations 11-13 with $k = 1, 2$, along with the previously determined values for x_{SRB} and b , are used to find expressions for the number of free dye molecules (N_f) in background, the number of liposomes (N_l), and the relative brightness of the SRB containing liposomes with respect to x_{SRB} ($\alpha = x_{Liposome}/x_{SRB}$). Ignoring the trivial solution of $\alpha = 1, f = g = 0$, these expressions are as follows:

$$\alpha = \frac{f}{g} - 1, \quad (14)$$

$$N_l = \frac{g}{\alpha(\alpha - 1)}, \quad (15)$$

$$N_f = \frac{\langle P \rangle}{x_{SRB}} - \frac{g}{\alpha - 1}, \quad (16)$$

where g and f are given by,

$$g = \frac{\langle \Delta P^2 \rangle - \langle P \rangle^2}{x_{SRB}^2} - \frac{\langle P \rangle}{x_{SRB}}, \quad (17)$$

$$f = \frac{\langle \Delta P^3 \rangle - 3\langle \Delta P^2 \rangle \langle P \rangle + 2\langle P \rangle^3}{x_{SRB}^3 / b} - \frac{\langle P \rangle}{x_{SRB}}. \quad (18)$$

2.2 Fluorescence correlation spectroscopy

FCS is a technique that, among other things, can be used to determine the concentration and size of diffusing fluorescent particles,⁷ based on measuring the second-order intensity autocorrelation function (ACF) of the fluorescence signal $F(t)$. Assuming $F(t)$ is a stationary process leads to a normalized ACF given by,

$$G(\tau) = \frac{\langle F(0)F(\tau) \rangle}{\langle F \rangle^2}. \quad (19)$$

Extracting useful information from an FCS measurement requires knowledge of the diffusion properties of the particles and the shape of the excitation volume. We assume a three-dimensional Gaussian excitation volume given by,

$$I(\vec{r}) = \exp\left(-\frac{2(x^2 + y^2)}{w_o^2}\right) \exp\left(-\frac{2z^2}{z_o^2}\right) \quad (20)$$

with particles undergoing Brownian motion in three dimensions. These assumptions have some deficiencies,⁸ but are appropriate for this work. The 3-D Gaussian excitation leads to the following expression for the ACF of a multi-species system⁷

$$G(\tau) - G(\infty) = \sum_k \frac{G_k(0)}{(1 + \tau/\tau_{D_k}) \sqrt{1 + \frac{w_o^2 \tau}{z_o^2 \tau_{D_k}}}} \quad (21)$$

where, τ_{D_k} is the k^{th} species diffusion time through the observation volume, $G(\infty)$ is the long time result for G having a theoretical value of 1, and $G_k(0)$ is related to the concentration and brightness of the k^{th} species.

Following Wohland *et al.*⁹ we report normalized FCS data, $g(\tau)$, such that $g(0) = 1$,

$$g(\tau) = \frac{1}{N_S} \sum_{i=1}^{N_S} \frac{G_i(\tau) - G_{i,\infty}}{G_i(0) - G_{i,\infty}}, \quad (22)$$

where N_S is the number of data samples measured and the standard error of $g(\tau)$ is given by,

$$E[g(\tau)] = \frac{1}{\sqrt{N_s}} \sqrt{\frac{1}{N_s - 1} \sum_{i=1}^{N_s} \left(\frac{G_i(\tau) - G_{i,\infty}}{G_i(0) - G_{i,\infty}} - g(\tau) \right)^2}. \quad (23)$$

The error in $g(\tau)$ is absent any systematic errors that may cause a change in the average number of particles between measurement sets which gives a more accurate estimate of the uncertainty. A fit of the experimental data, weighted for errors from eq. 23, extracts τ_D from which the diffusion coefficient and the average size of the fluorescent (spherical) particle can be found,

$$\tau_D = \frac{w_o^2}{4D} \quad (24)$$

$$D = \frac{k_B T_S}{6\pi\mu r}, \quad (25)$$

where D is the diffusion coefficient, k_B is Boltzmann's constant, T_S is the solution temperature, μ is the dynamic viscosity of the medium, and r is the radius of the diffusing particle.

2.3 Deadtime and afterpulsing

Deadtime and afterpulsing are two sources of error, usually associated with avalanche photodiodes (APDs), which can be accounted for in FCA measurements. The deadtime, T_{dead} , is the time, after a photodetection, before the detector is ready to detect another photon. Afterpulsing refers to spurious photon counts that occur after the detection of a real photon event. The deadtime corrected photon PDF, $\Pi'(P)$, in terms of the ideal photon PDF, $\Pi(P)$, (to first order in $\delta = T_{dead}/T$), is given by,¹⁰

$$\Pi'(P) = \Pi(P) + \delta[P(P+1)\Pi(P+1) - P(P-1)\Pi(P)] \quad (26)$$

and to first order in the afterpulsing probability, P_A , the afterpulsing corrected photon PDF, $\Pi^*(k)$, is given by¹¹

$$\Pi^*(P) = (1 - PP_A)\Pi(P) + (P-1)P_A\Pi(P-1). \quad (27)$$

Three conditions must be satisfied by $\Pi_m(P)$, the measured photon PDF,

$$\Pi_m(P) = \Pi'(P) \text{ for } P_A = 0, \quad (28)$$

$$\Pi_m(P) = \Pi^*(P) \text{ for } \delta = 0, \quad (29)$$

$$\sum_P \Pi_m(P) = 1. \quad (30)$$

Combining eqs. 26 and 27 using eqs. 28-30 gives,

$$\Pi_m(P) = \Pi(P) + \delta[P(P+1)\Pi(P+1) - P(P-1)\Pi(P)] + (P-1)P_A\Pi(P-1) - PP_A\Pi(P). \quad (31)$$

The corrected photocounting moments, $\langle P^n \rangle$, are extracted from the measured photocounting moments, $\langle P^n \rangle_m$, by inverting eq. 31 to first order in δ and P_A ,

$$\langle P \rangle = \langle P \rangle_m (1 - P_A - \delta) + \delta \langle P^2 \rangle_m, \quad (32)$$

$$\langle P^2 \rangle = \langle P^2 \rangle_m (1 - 2P_A - 3\delta) + 2\delta \langle P^3 \rangle_m + (\delta - P_A) \langle P \rangle_m, \quad (33)$$

$$\langle P^3 \rangle = \langle P^3 \rangle_m (1 - 3P_A - 6\delta) + 3\delta \langle P^4 \rangle_m + (4\delta - 3P_A) \langle P \rangle_m. \quad (34)$$

3. EXPERIMENT

3.1 Fluorescence microscopy

The experimental work is performed on a confocal fluorescence microscopy setup built on an inverted microscope. A frequency doubled Nd:YAG laser operating in continuous wave mode at 532 nm is sent through the back aperture of a $63\times$, 1.2 NA, water-immersion microscope objective. The laser beam underfills the back aperture of the objective to create a large excitation volume. The laser power sent to the microscope objective is approximately 500 μ W, and it is manually adjusted with polarization optics to eliminate intensity fluctuations on the minutes time scale. A chamber for holding solution is made by drilling a 1 cm hole through a microscope slide and sealing a #1.5 glass coverslip to the bottom of the slide using vacuum grease. 100 μ L of sample is placed into the hole and another coverslip is sealed over the hole with vacuum grease. Fluorescence light from the sample is focused down onto a 100 μ m pinhole and appropriate dichroic mirrors and optical filters direct the fluorescence light of interest onto the active area of an avalanche photodiode. Most photon arrivals create transistor-transistor logic (TTL) pulses that are sent to a peripheral component interconnect (PCI) hardware counting card.

The TTL pulses are counted and analyzed with a homemade software multi-tau correlator¹² having a temporal range from 4 μ s to 2 s. The software also bins the number of photons arriving within a $T = 16$ μ s integration time and creates a histogram of photon counts. The ACF and photon counting histogram is stored every 20 s. Typically, 40 data sets are collected for each sample from which the first three moments along with standard deviations are calculated. Deadtime and afterpulsing effects are corrected with eqs. 32-34. Values for δ and P_A are extracted using a method described elsewhere¹³ with typical values for δ and P_A ranging between 0.005 and 0.02. The standard deviation of each moment is propagated through eqs. 14-16 to arrive at the standard deviation for α , N_l , and N_f . The standard error is found by dividing the standard deviation by the square root of the number of measured data sets. Occasionally, large photon bursts occur from a cluster of liposomes diffusing through the laser beam. Any 20 s data set that leads to a value for either α , N_l , or N_f greater than 5 standard deviations from their respective means is discarded.

One difficulty with the hardware-counting card discussed elsewhere¹² is that limited memory capabilities can lead to software crashes during data taking. This problem was avoided with a program that creates a TTL pulse with an arbitrary delay time triggered on each arriving TTL pulse. If a second pulse arrives before the artificial pulse is finished, then that pulse is lost. This program allows for control over the detector deadtime, and it provides a way to verify eq. 31. Values of δ and P_A were measured for detector deadtimes ranging from 50 ns to 375 ns. The molecular brightness, x_{SRB} , was measured at different deadtime values from a 1 nmol/L solution of SRB in water. Figure 1 shows the corrected and uncorrected molecular brightness of the SRB molecules in water.

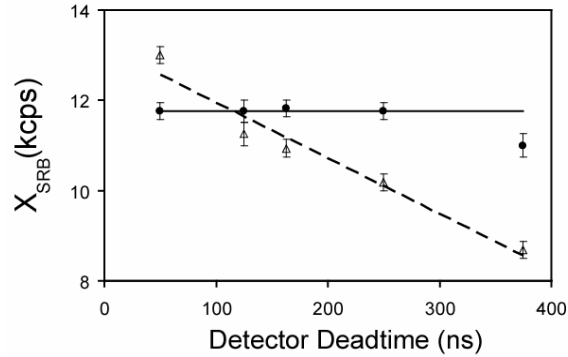


Fig. 1. The molecular brightness of SRB as a function of increasing detector deadtime. The uncorrected (open triangle with dashed line) and corrected (circle with solid line) values for the brightness parameter illustrate that, up to 250 ns, the deadtime and afterpulsing effects are corrected with a first order theory. All experiments in this report were performed with a deadtime setting of 145 ns which corresponds to $\delta = 0.009$ and $P_A = 0.005$.

Calibration experiments, with a 1 nmol/L solution of SRB in water, were performed daily and used to extract x_{SRB} .

$$x_{SRB} = \frac{\langle \Delta P^2 \rangle - \langle P \rangle}{\langle P \rangle}, \quad (35)$$

the geometric parameter b ,

$$b = \frac{x_{SRB}^2}{\frac{\langle \Delta P^3 \rangle}{\langle P \rangle} - 3x_{SRB} - 1}, \quad (36)$$

and the excitation volume, extrapolated from the zero value of $G(\tau)$,

$$V_{exc} = \frac{1.6}{G(0)/G(\infty) - 1} \times 10^{-15} L. \quad (37)$$

3.2 Liposome formation

Liposomes are prepared with a flow focusing technique¹ briefly described here. Established semiconductor electronic processing techniques such as photolithography and deep reactive ion etching are used to create a microfluidic channel network in silicon. A stream of lipids dissolved in isopropyl alcohol (IPA) is hydrodynamically focused in a microfluidic channel with two oblique aqueous buffer streams (fig. 2). Laminar flow conditions in the microchannel enable diffusive mixing in a direction normal to liquid flow streamlines. At a critical solvent-buffer ratio at the two liquid interfaces, the lipid monomers in the alcohol stream become insoluble and spontaneously self-assemble into spherical vesicles sequestering the surrounding aqueous fluid. SRB dye dissolved at various concentrations in the aqueous buffer allow for encapsulation of different concentrations of dye molecules within the liposomes. The liposomes translate downstream into the center channel and are collected at the center exit port. Liposomes of varying diameter result from changing the flow conditions in the microchannel. Non-encapsulated SRB dye is later

removed using a gel filtration column. The precise control of the flow field in a microchannel network produces liposome populations that are nearly monodisperse and of controlled size.

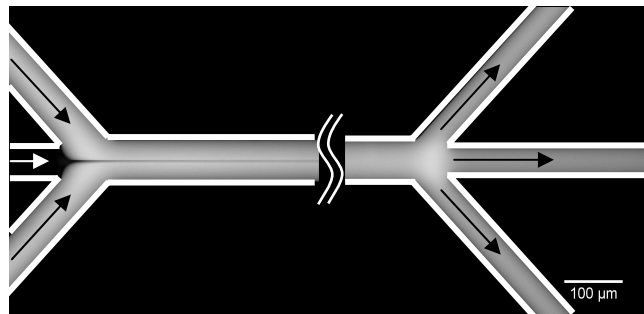


Fig. 2. A fluorescence image of the hydrodynamic focusing of the lipid-alcohol stream entering the center channel from the left with two oblique aqueous buffer streams containing SRB dye. Liposomes are collected from the middle channel on the right.

4. RESULTS

Two assumptions are required to use FCA in analyzing fluorescent liposome populations. First, the liposomes are considered pointlike *fluorescent* objects. FCS measurements show that the average diameter of the liposomes across all samples is between 50 nm and 100 nm, which translates into a liposome volume range between $0.65 \times 10^{-4} \text{ fL}$ and $5 \times 10^{-4} \text{ fL}$. Comparing these liposome volumes to the excitation volume found from FCS measurements, $(4.0 \pm 0.2) \text{ fL}$, shows that the first assumption is valid. Second, the effects associated with the Brownian motion of the encapsulated dye molecules are negligible. This assumption is justified with FCS measurements. Figure 3 shows $g(\tau)$ for a 1 nmol/L solution of SRB dye. The data is fit with the one-species version of eq. 21 which leads to a reduced χ^2 of 0.50.¹⁴

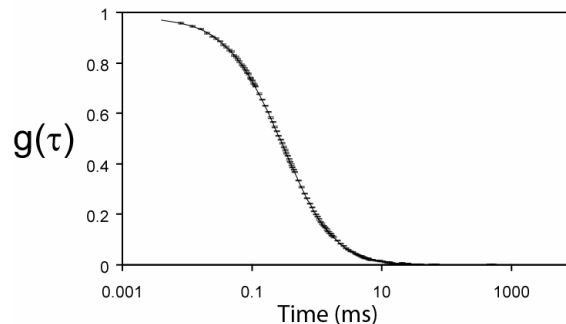


Fig. 3. Autocorrelation data (with error bars from eq. 23) of SRB dye at a 1 nmol/L concentration. The data is fit with only one component from eq. 12. The fit parameters are $(\tau_D, g(0), w_0/z_0) = (312 \text{ } \mu\text{s}, 0.40, 0.37)$ with a reduced χ^2 of 0.50.

FCS data from a sample of liposomes with an average relative brightness of $\alpha = 8.0$ is shown in fig. 4a. There appears to be no contribution from background dye. This is supported by a reduced χ^2 of 0.99 for a one species fit to the data. The Brownian motion of the encapsulated dye molecules also appears negligible although we note that the reduced χ^2 has doubled from the single dye molecule fit. Figure 4b shows $g(\tau)$ for the same liposome solution with 7.5 nmol/L of SRB added to the background. Assuming a single species fit leads to a reduced χ^2 value of 11.6 and a two species fit leads to a reduced χ^2 of 0.44. Figures 4a

and 4b and the corresponding χ^2 analysis suggest that when there is a negligible amount of background dye, then a one-component model that ignores the internal dynamics of the dye molecules encapsulated within the liposomes is sufficient. Therefore, if a one species model of FCS data leads to a reduced χ^2 value near 1, then the sample is analyzed assuming no background dye and only the first two cumulants of the photon PDF are required. If a two species model of FCS data gives a reduced χ^2 value near 1, then the sample is analyzed with the first three cumulants of the photon PDF.

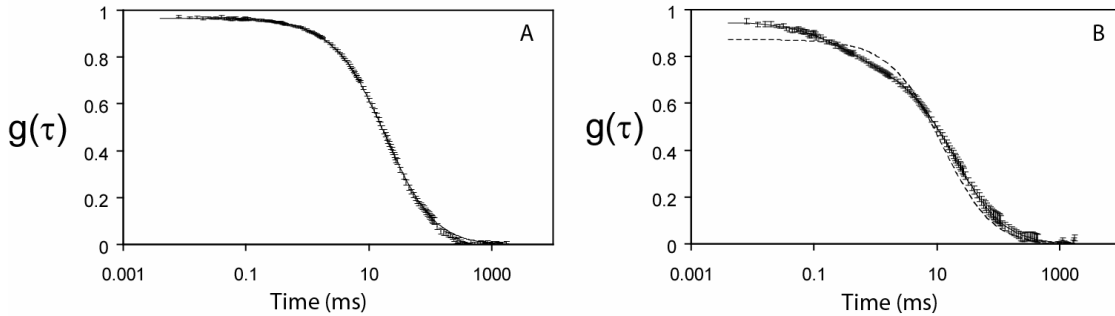


Fig. 4. (A) FCS data for a sample of liposomes with SRB encapsulated inside. A single species fit is assumed with parameters $(\tau_D, g(0), w_o/z_o) = (19.5 \text{ ms}, 0.34, 0.37)$ and a reduced $\chi^2=0.99$. Note that w_o/z_o is fixed by the 1 nmol/L free dye solution in fig. 3. (B) The same sample with 7.5 nmol/L background dye added. The dashed line is a best fit assuming a one-species model with parameters $(\tau_D, g(0), w_o/z_o) = (12.8 \text{ ms}, 0.87, 0.37)$ and a reduced $\chi^2=11.6$. The solid line is the best fit with a two-species model with parameters $(\tau_{D1}, g_1(0), \tau_{D2}, g_2(0), w_o/z_o) = (19.5 \text{ ms}, 0.76, 312 \mu\text{s}, 0.18, 0.37)$ and a reduced $\chi^2=0.44$. Note that τ_{D1} , τ_{D2} , and w_o/z_o are all fixed from previous fits. The average liposome diameter, calculated from (A) and eqs. 24, 25, and 37 is approximately 90 nm.

Three-cumulant FCA was performed on three different liposome samples over a period of two months. The long-time behavior of the liposome brightness (α), liposome concentration, and background dye concentration over this period is shown in fig. 5. Assuming a constant brightness of $\alpha = 8.6$ over the two-month period results in a reduced χ^2 of 1.6, suggesting that the liposome brightness remains stable. Notably, the liposome concentration decays while the background dye increases. One possible explanation is that the liposomes may be bursting upon contact with the container wall. Another possibility is that, over long periods, liposomes may fuse together and some dye could leak outside the membrane during this fusion process. In either case, more work needs to be done to explain these trends. Table 1 shows the long-term behavior of two other liposome samples over the same two-month period.

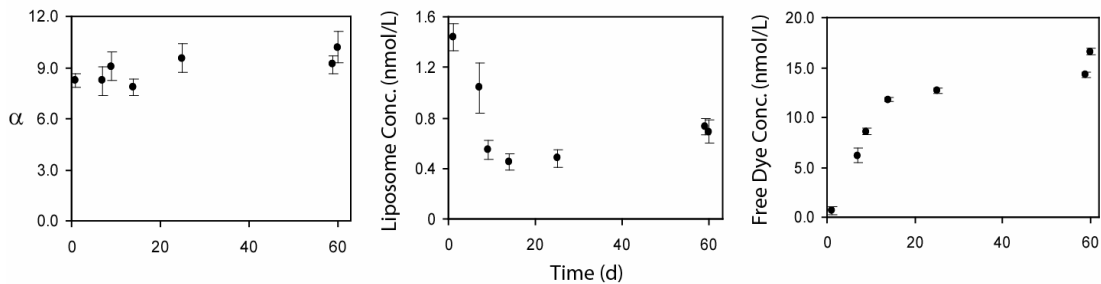


Fig. 5. The brightness, liposome concentration, and background dye concentration for one sample of liposomes measured over a period of two months. This particular sample saw a decrease in the liposome concentration and an increase in the background dye concentration while the average liposome brightness remained nearly constant.

Similar behavior in the liposome brightness and increased concentration of background dye is seen across all three samples. The concentration of liposomes seems stable, within the error bars, for the samples shown in the table.

Table 1. Two samples of liposomes measured over a two-month period. All concentrations listed here are in units of nmol/L. The number of data sets measured per sample is 30. The error bars are calculated using a method described in the text.

Date	Sample 1	Sample 2
2/6/2007	$\alpha = 5.05 \pm 0.70$ $c_{lip} = 0.19 \pm 0.04$ $c_{free} = 0.90 \pm 0.09$	$\alpha = 27.2 \pm 3.9$ $c_{lip} = 0.28 \pm 0.06$ $c_{free} = 5.79 \pm 0.68$
2/13/2007	$\alpha = 4.11 \pm 0.24$ $c_{lip} = 0.20 \pm 0.03$ $c_{free} = 1.18 \pm 0.07$	$\alpha = 23.5 \pm 2.0$ $c_{lip} = 0.26 \pm 0.03$ $c_{free} = 8.30 \pm 0.30$
4/6/2007	$\alpha = 5.84 \pm 0.70$ $c_{lip} = 0.24 \pm 0.06$ $c_{free} = 1.92 \pm 0.16$	$\alpha = 23.7 \pm 2.7$ $c_{lip} = 0.33 \pm 0.06$ $c_{free} = 13.7 \pm 0.5$

5. CONCLUSION

Liposome brightness values are reported relative to the brightness of free SRB molecules dissolved in water. If the brightness of the molecules inside the liposomes equals the free dye molecular brightness, then one could easily convert α to an encapsulation efficiency. This cannot be done at this time for two reasons. Small amounts of IPA may be contained within the liposomes, and the SRB molecules may be bound to the liposome membrane. Both effects alter the molecular brightness of SRB from its value in free solution. Further chemical analysis is required to determine the concentration of IPA within the liposomes, and polarization anisotropy measurements should address the membrane binding issue.

In summary, we characterized the long-term stability of liposomes prepared with flow-focusing technology. This characterization relied on several non-invasive, fluorescence fluctuation techniques. FCS was used to justify the FCA models and estimate the size of the liposomes. FCA was used to measure the liposome brightness, concentration, and the background dye concentration. It was found that the liposome brightness remains stable over a period of at least two months and that the concentration of the background seems to increase over this same period. More work is required in order to relate the liposome brightness to the encapsulation efficiency, but, even with relative brightness measurements, we may be able to optimize the liposome formation process.

ACKNOWLEDGEMENTS

We thank Brian Nablo and Samuel Stavis for helpful discussions and their interest in this project.

REFERENCES

1. A. Jahn, W. N. Vreeland, M. Gaitan, and L. E. Locascio, "Controlled vesicle self-assembly in microfluidic channels with hydrodynamic focusing," *J. Am. Chem. Soc.* 126, 2674-2675, (2004).
2. C-S Chen, J. Yao, and R. A. Durst, "Liposome encapsulation of fluorescent nanoparticles: quantum dots and silica nanoparticles," *J. Nanopart. Res.* 8, 1033-1038, (2006).
3. P. Rigler and W. Meier, "Encapsulation of fluorescent molecules by functionalized polymeric nanocontainers: investigation by confocal fluorescence imaging and fluorescence correlation spectroscopy," *J. Am. Chem. Soc.* 128, 367-373, (2006).
4. H. Qian and E. L. Elson, "Distribution of molecular aggregation by analysis of fluctuation moments," *Proc. Natl. Acad. Sci. U.S.A.* 87, 5479-5483, (1990).
5. H. Qian, "On the statistics of fluorescence correlation spectroscopy," *Biophys. Chem.* 38, 49-57, (1990).
6. B. Wu and J. D. Mueller, "Time-integrated fluorescence cumulant analysis in fluorescence fluctuation spectroscopy," *Biophys. J.* 89, 2721-2735, (2005).
7. S. T. Hess, S. Huang, A. A. Heikal, and W. W. Webb, "Biological and chemical applications of fluorescence correlation spectroscopy: a review," *Biochemistry* 41, 697-705, (2002).
8. S. T. Hess and W. W. Webb, "Focal volume optics and experimental artifacts in confocal fluorescence correlation spectroscopy," *Biophys. J.* 83, 2300-2317, (2002).
9. T. Wohland, R. Rigler, and H. Vogel, "The standard deviation in fluorescence correlation spectroscopy," *Biophys. J.* 80, 2987-2999, (2001).
10. K. A. O'Donnell, "Correction of dead-time effects in photoelectric-counting distributions," *J. Opt. Soc. Am. A* 3, 113-115, (1986).
11. L. Campbell, "Afterpulse measurement and correction," *Rev. Sci. Instrum.* 63, 5794-5798, (1992).
12. D. Magatti and F. Ferri, "25 ns software correlator for photon and fluorescence correlation spectroscopy," *Rev. Sci. Instrum.* 74, 1135-1144, (2003).
13. L. N. Hillesheim and J. D. Muller, "The photon counting histogram in fluorescence fluctuation spectroscopy with non-ideal photodetectors," *Biophys. J.* 85, 1948-1958, (2003).
14. P. R. Bevington and D. K. Robinson, *Data Reduction and Error Analysis for the Physical Sciences*, WCB/McGraw-Hill, New York, 1992.